Dynamics of tetrahedral networks: Amorphous Si and Ge

N. Maley*
Department of Physics, Penn State University, University Park, Pennsylvania 16802

D. Beeman
Department of Physics, Harvey Mudd College, Claremont, California 91711

J. S. Lannin
Department of Physics, Penn State University, University Park, Pennsylvania 16802
(Received 6 May 1988)

Experimental data are reported for depolarized and fully polarized components of the Raman spectra of variably ordered states of *a*-Ge and *a*-Si films. These spectra are compared to theoretical Raman calculations for relaxed Polk-model-derived structures with different degrees of bond-angle disorder. In addition, the experimental and theoretical densities of states of *a*-Ge in highly ordered and disordered states are reported. The Raman spectra for the fully polarized component are found to yield good agreement at high frequencies, as well as the observed trend of decreased width with increasing bond-angle order. At low frequencies the theoretical spectra are more intense than that observed experimentally, indicating limitations of the three-parameter phenomenological Raman polarizability model. The depolarized Raman component may, in contrast, be fitted reasonably well with a fixed ratio of the $\tilde{D}_1$ and $\tilde{D}_2$ mechanisms at intermediate and higher energies. The two-parameter lattice-dynamical calculation of the density of states also yields good agreement with experiment, except at intermediate frequencies, where a somewhat more intense scattering is observed. A comparison of experimental and theoretical results allows estimates of the bond-angle disorder in *a*-Ge and *a*-Si to be obtained. The results are consistent with estimates based on radial-distribution-function and calorimetry studies.

I. INTRODUCTION

Inelastic probes such as Raman scattering provide a high-resolution method for studying the vibrational dynamics and bonding of amorphous solids. This has allowed variations in structural order to be explored in tetrahedral amorphous Ge and Si under modifications of deposition and annealing conditions, as well as in interfacial bonding associated with superlattice structures.[1-4] Such measurements are of additional importance to understanding the relation of structure to other physical properties of amorphous solids which depend on local-order variations. Given the difficulties of directly determining small variations in the radial distribution function (RDF), these measurements provide a high-sensitivity probe of short-range order (SRO).

The absence of periodicity in amorphous solids implies that the Raman scattering tensor is related to a coupling parameter weighted vibrational density of states. A more detailed analysis employing a bond-polarizability model indicates that the Raman scattering components are related to three distinct mechanisms, $\tilde{D}_j$.[5,6] Although early depolarization measurements suggested that one of these, $\tilde{D}_3$, vanished,[5] subsequent studies indicated that this was not the case.[7] Recent theoretical calculations[2] on models of *a*-Si indicated that variations in structural order were manifest in the Raman spectra, with emphasis on the variations in the spectra from $\tilde{D}_2$. In the present work more detailed experimental and theoretical results are presented which indicate the importance of all three mechanisms. It is shown that the fully polarized, HH-$(4/3)VH$, spectrum is also a function of structural order and yields direct information about $\tilde{D}_3$ within the current model. A comparison between experiment and theory for the fully polarized and depolarized Raman components allows a quantitative relation between the TO band linewidths and the bond-angle disorder to be obtained. The results indicate a somewhat larger minimum value of the width of the bond-angle distribution than previous estimates based on the $\tilde{D}_2$ mechanism alone,[2] but in accord with other estimates based on structural and optical data.[1] Recent estimates obtained from an analysis of differential scanning calorimetry, in which structural relaxation is assumed to be a quadratic function of bond-angle variance, yield similar results for SRO variations.[8]

Information about the vibrational dynamics and the role of structural order may also be studied by inelastic neutron scattering measurements. In the case of elemental materials the modified dynamical structure factor $G(Q,E)$ may be appropriately averaged over a range of Q values, after multiphonon and multiple-scattering background estimates, to obtain the phonon density of states $G(E)$.[9,10] Such measurements on two states of *a*-Ge prepared so as to maximize their differences in order have indicated the sensitivity of $G(E)$ at high phonon energy to SRO.[11] Although a number of previous calculations of $G(E)$ have been performed in *a*-Ge and *a*-Si, it has not been possible to obtain a meaningful comparison between

theory and experiment, given the limited number of samples studied and the absence of information about their SRO. In the present study information about SRO is provided by a number of comparisons between experiments and theory that provide for a more useful evaluation of the dynamics of *a*-Si and *a*-Ge. Implicit in all calculations of $G(E)$ in amorphous semiconductors to date has been the assumption that the nearest- and next-nearest-neighbor force constants do not vary spatially. That is, quantitative disorder which is known to be present is neglected. While the present theoretical results utilizing this assumption indicate relatively good agreement between experiment and theory, some differences in peak widths are observed which suggest the possible need to consider the influence of quantitative disorder in *a*-Si and *a*-Ge.

II. EXPERIMENT

Raman measurements were performed on low-pressure rf-sputtered *a*-Si and *a*-Ge films at 300 K. Selected measurements were also performed on evaporated *a*-Ge and chemical vapor deposited *a*-Si films. Reported here are a subset of the data relevant to a comparison with theory. Inelastically scattered radiation excited with a 5145-Å Ar laser was analyzed with a Spex Industries third monochromator system and partially smoothed by an instrument controlling microcomputer. From *VH* and *HH* spectra the fully polarized HH-$(4/3)VH$ spectra were obtained after subtraction of stray light background. Although these Stokes spectra are primarily associated with the first-order Raman process, small second-order scattering may also contribute.[1]

The phonon density of states was obtained for two large samples of highly ordered (HO) and highly disordered (HD) *a*-Ge prepared by high rate dc triode, magnetron, and rf diode sputtering, respectively.[11] Measurements of $G(Q,E)$, the modified dynamical structure factor, were employed to obtain $G(E)$ after averaging over neutron momentum transfers between 4 and 7 $Å^{-1}$. The procedure for background subtraction and corrections for multiple phonon and neutron scattering have been reported elsewhere.[10] Table I indicates the conditions of formation for the Raman and neutron samples.

III. THEORETICAL MODELS AND RAMAN CALCULATIONS

In order to systematically study the effects of structural disorder on the Raman spectra, two series of structural models were created, based upon the 500-atom and 519-atom models of Polk and Boudreaux.[12,13] The original 500- and 519-atom models had rms bond-angle deviations of 6.7° and 7.3°, respectively, with calculated RDF's which are in relatively good agreement with various experimental results for *a*-Ge.[14,15] However, the width of the second peak in the RDF obtained on sputtered and evaporated *a*-Ge ($\sim 9.5°-10.5°$) is much greater than that obtained from these models, indicating a need to increase the amount of bond-angle distortion. The models were first given random atomic displacements, resulting in large bond-angle variations of about $\pm 20°$. They were then relaxed using the method of Steinhardt *et al.*[16] At various times the relaxation procedure Was interrupted to obtain models with different rms bond-angle distributions ranging from $\sim 7°-13°$. This procedure approximately fixes the dihedral angle distribution and local topology of the system to be near that of the initial model. For these models this implies a dihedral angle distribution with approximate ratios of two and three for staggered versus eclipsed bonds for the 519- and 500-atom models, respectively. Although a recent evaluation[17] sug-

TABLE I. Preparation parameters and "TO" peak width in measured and reduced VH Raman spectra for the *a*-Si and *a*-Ge samples used for comparison with theory. T_d is the deposition temperature. CVD means chemical-vapor deposition.

Film code	Preparation method	Conditions P_{Ar} (mTorr)	Conditions T_d (°C)	VH TO peak width in measured spectra (cm^{-1})	VH TO peak width in reduced spectra (cm^{-1})
			a-Si		
a	CVD		650	83	78
b	rf diode	7	500	105	94
c	rf diode	7	200	140	110
d	rf diode	7	30	160	120
			a-Ge		
a	Evaporation		25 (300)[a]	57	46
b	Evaporation		25	69	55
c	rf diode	30	200	82	63
d	rf diode	7	30	100[b]	77
HO	rf magnetron	5	150	65	56
HD	rf diode	7	−5	97[b]	71

[a]Annealed at 300 °C.

[b]Value obtained by extrapolation of LO region shoulder.

gests that a more uniform, broader distribution of dihedral angles may specify the structure of *a*-Ge and *a*-Si, this should not significantly influence the present theoretical trends obtained here. This is also a consequence of the dominance of first- and second-neighbor interactions on most of the vibrational and Raman spectral features. The actual formation of amorphous materials of variable network order may be influenced by the effects of growth kinetics on different topologies. This may occur, for example, as deposition conditions are modified. Annealing of as-deposited structures is more likely to result in smaller variations in topology.

The Raman tensor $D_{i\alpha}^{\mu\nu}$ may be represented in a bond-polarizability model as a coherent sum of three contributions j with relative weighting factors B_j,

$$D_{i\alpha}^{\mu\nu}=\sum_j B_j(D_{i\alpha}^{\mu\nu})_j \ . \tag{1}$$

Here the ith atom has displacement components α that yield polarizability fluctuations for incident and scattered electric fields along μ and ν directions, respectively. The equation-of-motion method[6] was utilized to calculate Raman intensities from initial displacements which are proportional to the three independent Raman components,[5,6] $(D_{i\alpha}^{\mu\nu})_j$. These three distinct mechanisms arise under the assumption of cylindrical symmetry of the bond polarizability, and translational and inversion spatial symmetry considerations.[5] Depolarized, *VH* scattering involves six components of the symmetric Raman tensor, $D_{i\alpha}^{\nu\beta}=D_{i\alpha}^{\beta\nu}$, with i equal to 1 and 2, whereas the fully polarized, *HH*-(4/3)*VH* component is a function of three identical diagonal elements of $\tilde{D}_3$. Averages over these elements were employed to obtain the scattering contributions, $\tilde{D}_j$. For the $\tilde{D}_3$ component the statistical fluctuations are increased over that of $\tilde{D}_1$ or $\tilde{D}_2$ due to the smaller sampling. The first-order Raman Stokes intensities, $I^{(1)}(\omega)$ are then obtained from

$$I_{\rm DP}^{(1)}(\omega)=\tfrac{3}{4}[(B_1\tilde{D}_1)^2+(B_2\tilde{D}_2)^2](n+1)/\omega \ , \tag{2}$$

$$I_{\rm FP}^{(1)}(\omega)=[(B_3\tilde{D}_3)^2](n+1)/\omega \ . \tag{3}$$

The quantities in square brackets are related to the average mode-independent, but frequency-dependent coupling parameters.

$$\tilde{C}_\delta^{(1)}(\omega)=I_\delta^{(1)}(\omega)\frac{\omega}{(n+1)}\Big/G(\omega) \ , \tag{4}$$

where $E=\hbar\omega$ and $\delta=VH$ or *HH*-(4/3)*VH*, for the depolarized (DP) and fully polarized (FP) components, respectively. Physically, the $\tilde{D}_1$ contribution is associated with stretchlike motions and primarily contributes to the high-frequency scattering. In contrast, $\tilde{D}_2$ and $\tilde{D}_3$ have substantial bend and stretch character. While $\tilde{D}_2$ and $\tilde{D}_3$ vanish for tetrahedral symmetry, D_1 does not.

Implicit in Eq. (2) is the assumption that the individual $\tilde{D}_j$ terms add incoherently for j. An estimate of the effect of coherency was obtained by weighting the initial displacements in the equation-of-motion by the estimated B_1 and B_2 factors that yielded a best fit between the experimental spectrum of sample *a* and that of model *B* discussed below. The theoretical *VH* Raman spectrum obtained in this manner indicated little change in the low- and intermediate-frequency bands. For the high-frequency TO band the theoretical spectrum was found to narrow slightly. As this yielded poorer agreement with experiment, the simpler incoherent approximation was employed for the $\tilde{D}_j$ contributions. The appreciable similarity of the results for the 500- and 519-atom models allows a reduction of statistical fluctuations by an average of their respective results. This simplicity emphasizes for *a*-Ge and *a*-Si the lack of sensitivity to the dihedral angle distribution and the predominance of short-range order noted in previous studies.

A two-parameter Born model was employed to calculate the vibrational densities of states and Raman spectra. In these calculations the ratio of the Born parameters β/α was taken as 0.143, in agreement with a fit to crystalline- (*c*-) Si and *c*-Ge elastic constants,[18] rather than the value of 0.222 used previously.[2] This yields improved agreement with the low- and high-frequency bands of the experimentally determined spectra. Figure 1 shows the density of states of a 525-atom cluster model of *c*-Ge computed with $\beta/\alpha=0.143$ compared with the neutron scattering results of Nelin and Nilsson.[19] Except for differences in the lowest frequency TA peak, the agreement is very good for a two-parameter model.

IV. EXPERIMENTAL AND THEORETICAL RESULTS

A. Experiment

The variation of the *VH* Raman spectra for sets of *a*-Ge and *a*-Si films of variable order is shown in Fig. 2. For comparisons with the theoretical results, the spectra have been reduced by dividing the Raman intensity by $(n+1)/\omega$. It is important to emphasize that these reduced spectra, while convenient for comparison with the theoretical results of Figs. 3 and 4, do not yield a good representation of the form of the density of states. This is a consequence of the significant coupling parameter increase with frequency.[20] The reduced spectra also less clearly indicate the changes in the TO to TA intensity with structural order.

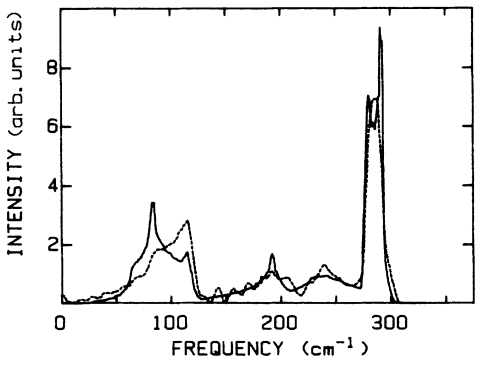

FIG. 1. Phonon spectra of *c*-Ge: Theoretical result with $\beta/\alpha=0.143$ (— — —) and experiment (——, from G. Nelin and G. Nilsson, Ref. 19).

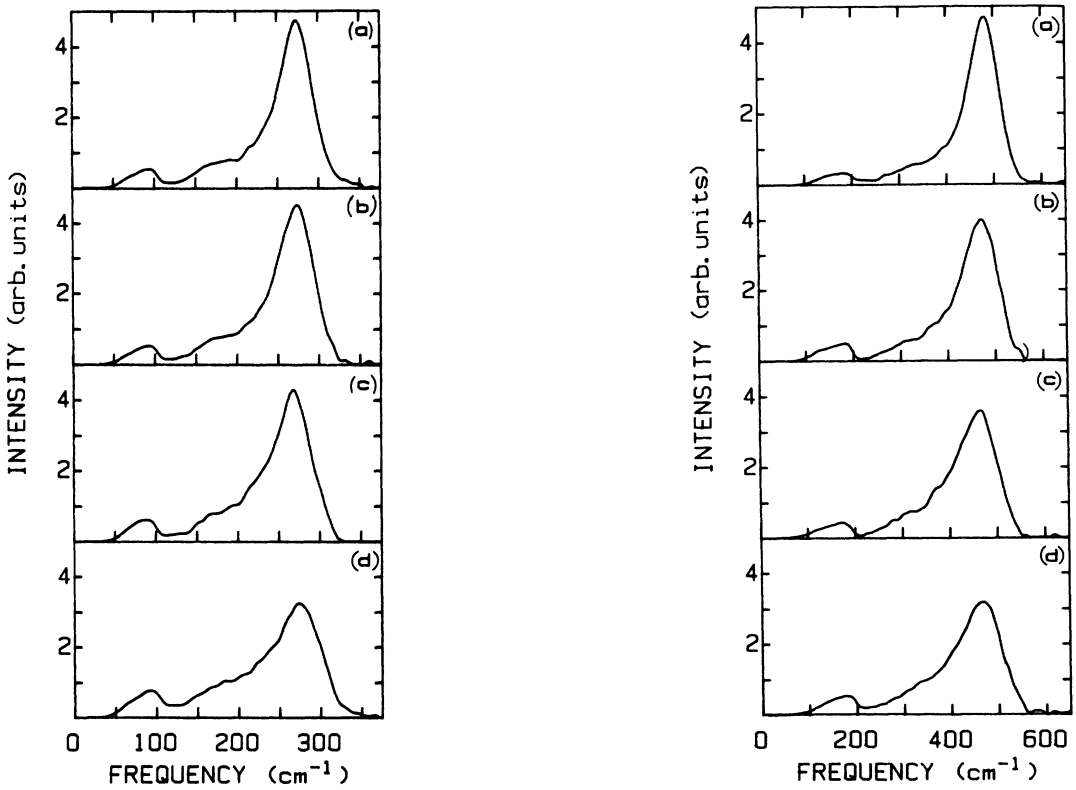

FIG. 2. Experimental VH spectra in reduced form for most ordered (a) through most disordered (d). *a*-Si, right panel; *a*-Ge, left panel.

As noted earlier, the primary variation in the *VH* Raman spectra is an increased width of the high-frequency TO band and a relative decrease in TO/TA band intensities with enhanced bond-angle disorder.[1] The *HH*-(4/3)*VH* component spectra of *a*-Ge and *a*-Si, shown in Fig. 5, indicate similar trends as well as enhanced scattering at intermediate frequencies. These spectra also indicate somewhat greater relative TA scattering. The rather similar results obtained for both *a*-Si and *a*-Ge films are consistent with earlier *VH* and *HH* spectral variations with structural order, as well as with corresponding changes in the optical gap.[1] Table I indicates the TO full widths at half maximum intensity of the measured as well as reduced spectra of Fig. 2.

It is useful to note that the depolarization ratio, I_{VH}/I_{HH}, has a relatively constant value for the TO peak of 0.55 ± 0.05 for the various *a*-Ge and *a*-Si samples studied. This implies from Eqs. (2) and (3) that the relative contribution of the $\tilde{D}_3$ term to *HH* scattering is $\sim 25\%$ of the total. This emphasizes the point that *HH* or polarization unanalyzed Raman spectra have significant contributions from this mechanism.

B. Theory

The theoretically obtained $\tilde{D}_j$ components for a set of structural models are shown in Figs. 3 and 4 after averaging the 500- and 519-atom results. An analysis of the distribution of bond angles, $P(\theta)$, indicates a non-Gaussian form, particularly for large-angle deviations of low sta-

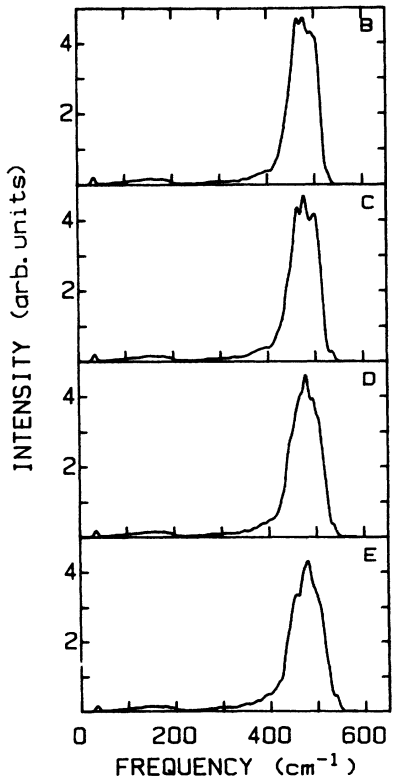

FIG. 3. Calculated Raman spectra for mechanism 1 on a similar intensity scale for models *B* through *E* on *a*-Si frequency scale.

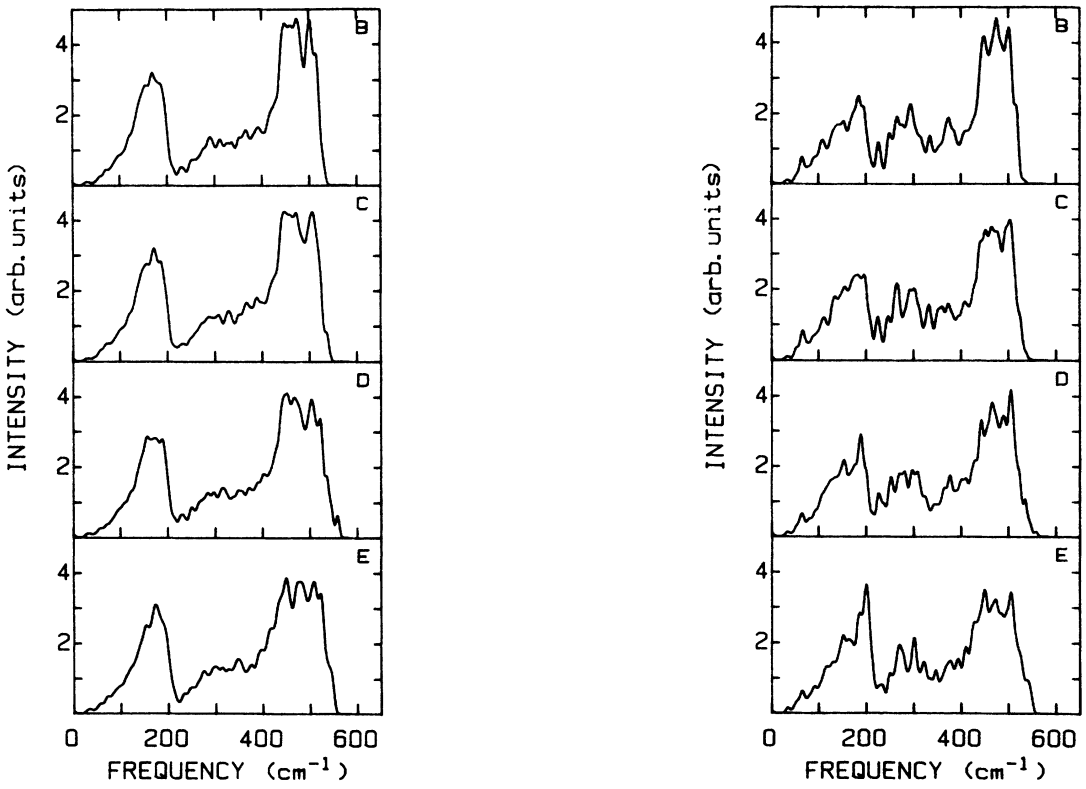

FIG. 4. Calculated *a*-Si Raman spectra for mechanism 2 for models *B* through *E* on a similar intensity scale (left panel) and mechanism 3 (right panel).

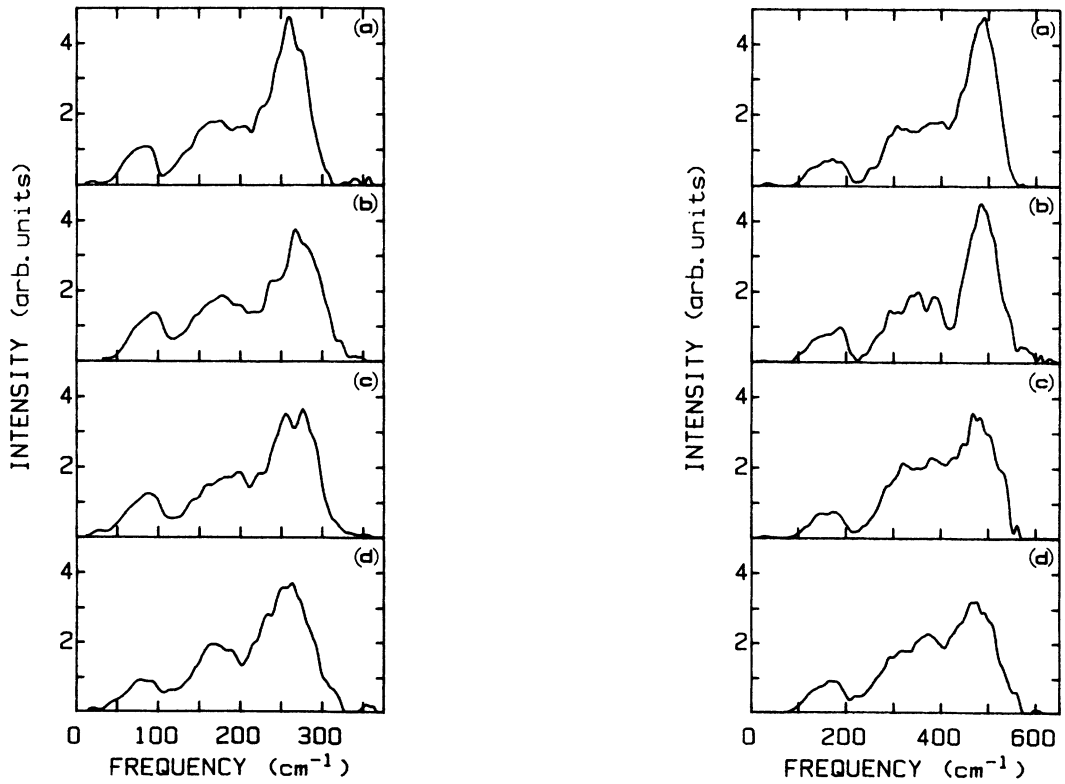

FIG. 5. Experimental *HH*-(4/3)-*VH* spectra in reduced form for most ordered (a) through most disordered (d). *a*-Ge, left panel; *a*-Si, right panel.

tistical weight. A least-squares fit to Gaussian distributions yields an effective Gaussian deviation, $\Delta\theta_G$, which is smaller than the root-mean-square value, $\Delta\theta_{\rm rms}$, of $P(\theta)$. This is indicated in Table II which exhibits an increase between $\Delta\theta_{\rm rms}$ and $\Delta\theta_G$ as the distribution broadens with disorder. For comparisons with the RDF and Raman spectra both parameters are employed. Previous studies and RDF analysis have implicitly assumed Gaussian behavior.

As Figs. 3 and 4 indicate, all three mechanisms show an increase in their TO peak width with increasing bond-angle distortion. Mechanism $\tilde{D}_1$, which contributes mainly to the TO peak, has a higher total integrated intensity which is essentially independent of structural disorder. In contrast, Table II indicates that $\tilde{D}_2$ and $\tilde{D}_3$, which vanish in the limit of perfect tetrahedral symmetry, yield an increasing contribution to the total intensity, and hence to the TA peak, with increasing disorder. An analysis of the scattering intensity for the $\tilde{D}_2$ and $\tilde{D}_3$ mechanisms indicates that their integrated intensity increases approximately as $(\Delta\theta_{\rm rms})^2$. This simple result may be seen to arise as a consequence of small displacements of vectors from atoms to their neighbors that deviate from perfect tetrahedral symmetry. It may be shown that the total integrated intensity calculated from the equation of motion method is proportional to the sum of the squares of the initial displacements $x_{i\alpha}$, which are given by the Raman tensor components $D_{i\alpha}^{\mu\nu}$. For $\tilde{D}_2$ and $\tilde{D}_3$, these are proportional to the sum of the vectors between the ith atom and its four bonded neighbors,[5,6] which vanishes in the limit of perfect tetrahedral symmetry. In particular, if the direction α in Eq. (1) is taken for convenience to be along that of one of the bonded neighbors, the deviation from tetrahedral symmetry factor takes the form

$$\sum_{\Delta} r_{\Delta}^{\alpha}(i) = r_0 \left[1 + \sum_j \cos\theta_j \right] , \tag{5}$$

where j labels the other three neighbors of distances $r_\Delta(j)$ and θ_j represents their bond angles with the vectors $r_\Delta^\alpha(i)$ (This neglects any small spread in bond length.) If $\theta_j = \theta_0 + \Delta\theta_j$, where $\Delta\theta_j$ is the deviation from the tetrahedral value θ_0, then

$$\sum_{\Delta} r_{\Delta}^{\alpha}(i) = -r_0 \sin\theta_0 \sum_j \Delta\theta_j \tag{6}$$

for small $\Delta\theta_j$. If the distribution of $\Delta\theta_j$ values is symmetric about zero, the mean-square initial displacement $\langle x_{i\alpha}^2(0)\rangle_{\rm av}$ is then proportional to $\langle(\Delta\theta_j)^2\rangle_{\rm av}$. An evaluation of Raman intensities in the equation-of-motion method then indicates that the contributions from $\tilde{D}_2$ and $\tilde{D}_3$ are also quadratic functions of $\Delta\theta_{\rm rms}$.

The dependence of the $\tilde{D}_2$ and $\tilde{D}_3$ contribution on $\Delta\theta_{\rm rms}$ implies that the Raman intensity components more strongly weight deviations from tetrahedral behavior. This parallels the quadratic dependence of the local strain-free energy on bond-angle deviations. In contrast, structural studies have often tended to emphasize in the analysis of the rdf the e^{-1} intensity of the second-neighbor peak and thus the effective Gaussian deviation of the bond angle.

V. COMPARISON OF EXPERIMENT AND THEORY

A. Raman scattering

The relative contribution of the $\tilde{D}_1$ and $\tilde{D}_2$ mechanisms to the experimental *VH* spectrum can, in principle, be obtained by taking linear combinations of the former. For the $\tilde{D}_3$ mechanism, a direct comparison is possible as seen from Eq. (3). In comparing experiment to theory, it is desirable to accurately know the structure of the films studied. It has not been possible, however, to accurately obtain differences in the RDF's of *a*-Ge film with the accuracy required. Estimates of the effective Gaussian deviation in bond angle for *a*-Ge films have been obtained from a comparison of optical gap, Raman scattering TO width, and RDF measurements. The results suggested a

TABLE II. Bond-angle distribution width and integrated intensity for the different mechanisms (Mech.) for various structural models.

Model	$\Delta\theta$ rms	$\Delta\theta$ G (deg)	Integrated intensity Mech. 1	Mech. 2 (arbitrary units)	Mech. 3
519	7.28	7.20	151.0	3.76	17.3
519*A*	9.11	8.61	147.5	7.09	29.9
519*B*	10.10	9.34	144.9	9.37	42.1
519*C*	10.98	9.78	145.0	11.1	50.0
519*D*	12.08	11.10	140.3	14.8	66.5
519*E*	13.02	11.52	136.0	16.9	75.8
500	6.68	6.51	151.0	3.42	15.4
500*A*	9.09	8.74	146.0	6.65	17.3
500*B*	10.00	9.43	143.7	8.43	37.9
500*C*	10.94	10.00	141.0	10.5	47.3
500*D*	12.00	10.11	137.1	13.5	60.9
500*E*	13.00	11.51	133.3	17.0	76.7

range of $\Delta\theta_G \simeq 9°-11.5°$.[1,21] These results also suggest from Table I that models B and E are the most reasonable ones for comparison with our most and least ordered a-Ge samples a and d, respectively. The estimated $\Delta\theta_G$ values neglect possible contributions from third or higher bonded neighbors to the second RDF peak $J_2(r)$ and are thus *lower* limits. An analysis of model B indicates little contribution of $J_3(r)$ to the lower portion of the second RDF peak. A small contribution of $J_3(r)$ in model E implies that sample d may have somewhat greater disorder than model E.

An alternative semiquantitative approach to defining structural order in a-Ge samples $a-d$ would be to use a fit to the theoretical $\tilde{D}_3$ spectra to estimate the bond-angle variance. Differences exits, however, between the theoretical and the experimental FP spectra that limit an accurate estimate of bond-angle disorder. It has been found, however, that a comparison between both the experimental and theoretical VH and FP spectra yields a good correspondence if models B and E are compared to the most and least ordered spectra of a-Ge and a-Si. As discussed below, this allows the bond-angle disorder in other samples to be estimated. Shown in Figs. 6(b)–9(b) is the area normalized comparison between the FP reduced Raman spectra for the a and d samples of a-Si and a-Ge to that of models B and E, respectively. At intermediate and higher frequencies the correspondence is good between experiment and theory. With increasing disorder the theoretical spectra indicate the experimental trends of broadening of the TO band and the decrease in the TO intensity relative to that at lower frequencies. The presence of greater local fluctuations in frequency of the theoretical spectra, as noted above, is due to larger statistical noise for this Raman component. For the lower-frequency TA band the experimental and theoretical spectra differ substantially in intensity, the latter being more intense. This difference, which is clearly outside experimental error, suggests limitations on the present Raman theory for the FP component. As the current theory assumes a single-bond polarizability with cylindrical symmetry, it is reasonable to consider removal of this constraint to include second-neighbor effects on the po-

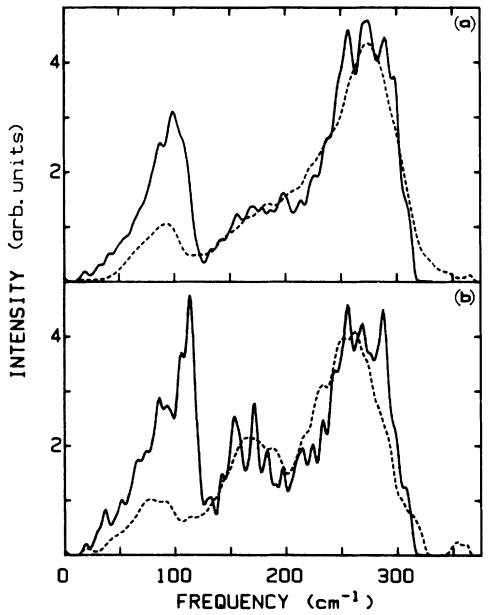

FIG. 7. Comparison of VH (a) and HH-(4/3)VH (b) reduced spectra for the most ordered Ge film (— — —) and model E (——).

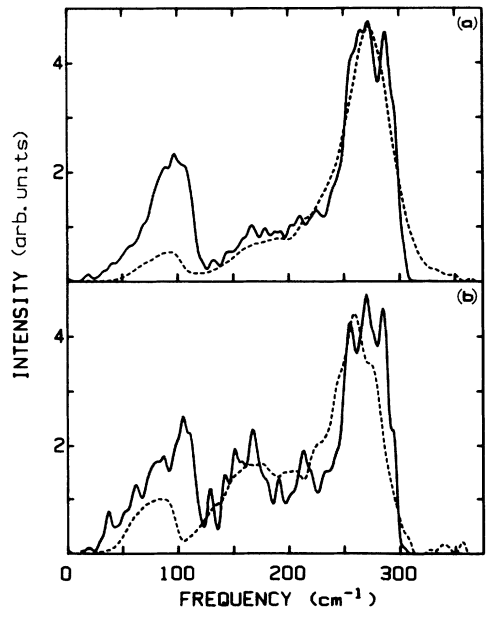

FIG. 6. Comparison of VH (a) and HH-(4/3)VH (b) reduced spectra for the most ordered Ge film (— — —) and model B (——).

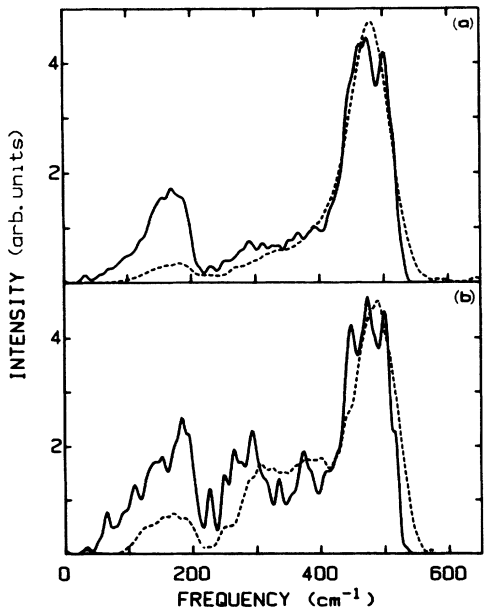

FIG. 8. Comparison of VH (a) and HH-(4/3)VH (b) reduced spectra for the most ordered Si film (— — —) and model B (——).

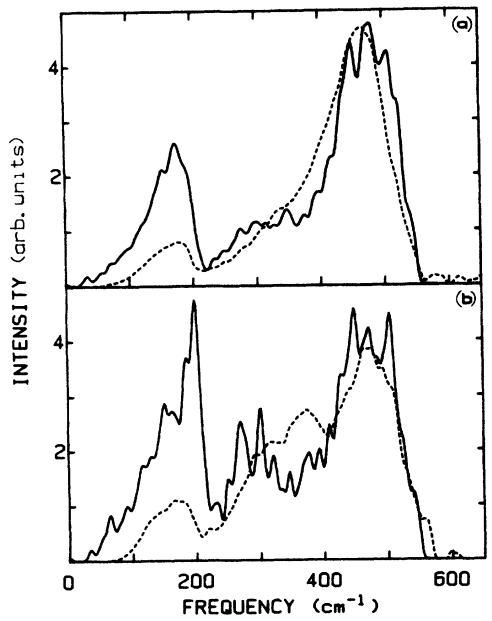

FIG. 9. Comparison of *VH* (a) and *HH*-(4/3)*VH* (b) reduced spectra for the most disordered Si film (— — —) and model *E* (——).

larizability. That this might improve agreement with experiment is plausible, given that the low-frequency region involves bond-bending motions. Support for this is provided by inelastic neutron measurements of the Q dependence of $G(Q,E)$ for the TA band. Here the oscillatory behavior at low Q indicates dynamical correlations beyond nearest neighbors.[11] The use of an additional FP parameter, including its possible coherency effects, would clearly result in a loss of simplicity present in the single-parameter theory.

In contrast to the FP spectra, the *VH* Raman component requires criteria in terms of a best fit to a linear combination of $\tilde{D}_1$ and $\tilde{D}_2$ mechanisms. Substantial differences in the ratio of $(B_1/B_2)^2$ result, for example, if the fit is made to the peak intensities of the TA and TO peaks versus optimizing the agreement at intermediate and higher frequencies. These differences were necessary to consider as it was not found possible to fit the form of the Raman spectra over the entire spectral range obtaining good agreement for both the TA- to TO-intensity ratio and the high- and intermediate-frequency band shapes. The latter fitting choice was employed based on the observation that the FP component does not agree with experiment and that limitations on the Raman theory more likely occur at lower frequencies. Figures 6(a) and 9(a) compare the *VH* Raman spectra of samples *a* and *d* of *a*-Ge and *a*-Si to weighted contributions from models *B* and *E*, respectively. The spectra are area normalized for the region above the minimum between TA and LA bands. As can be seen from the comparison the fit obtained is relatively good at intermediate and higher frequencies and follows the trends noted for the FP component for increasing disorder on the TO bandwidth and relative intensity. With this fitting procedure the TA band intensity is significantly lower in the experimental

TABLE III. Relative integrated reduced Raman spectral contributions are weighting factors for films *a* and *d*.

Sample	Ge *a*	Ge *d*	Si *a*	Si *d*
$I_{r(3)}/I_{r(1)}$	5.9	10.1	2.9	5.1
$({}_2B/{}_1B)^2$	87.5	87.5	43.7	43.7
$I_{r(2)}/I_{r(3)}$	2.35	2.5	2.0	2.3
$({}_2B/{}_3B)^2$	10.9	10.9	9.8	9.8

spectra. Table III indicates the values of $(B_1/B_2)^2$ obtained for the *a* and *d* samples of *a*-Ge and *a*-Si. Also shown in Table III is the ratio of the integrated reduced intensity ratios $I_{r(i)}/I_{r(j)}$. It is not known whether $(B_1/B_2)^2$ is a function of disorder. Rather than introduce an additional fitting parameter, we have chosen to keep it fixed and been able to obtain a reasonable fit to the spectra of *a*-Ge and *a*-Si. This fitting procedure yields an approximate factor of 2 increase in the contribution of the disorder-induced mechanism $\tilde{D}_2$ relative to the allowed $\tilde{D}_1$ mechanism with increasing disorder. For *a*-Ge the ratio of $\tilde{D}_2$ to $\tilde{D}_1$ contributions is found to be approximately a factor of 2 smaller for both samples relative to *a*-Si. Figures 10 and 11 indicate the relative contribution to the $\tilde{D}_2$ and $\tilde{D}_1$ mechanisms for the theoretical *VH* spectra of Figs. 6–9. For this fitting procedure, the results indicate that the $\tilde{D}_1$ contribution may not be excluded from an analysis of the spectra as was done in an earlier study.[5]

If the comparison between the *VH* experimental and theoretical reduced spectra is made using a criterion that requires a best fit to the TA and TO intensities, the same trend in the coefficients is observed both with increasing disorder and in the comparison with *a*-Ge and *a*-Si. This

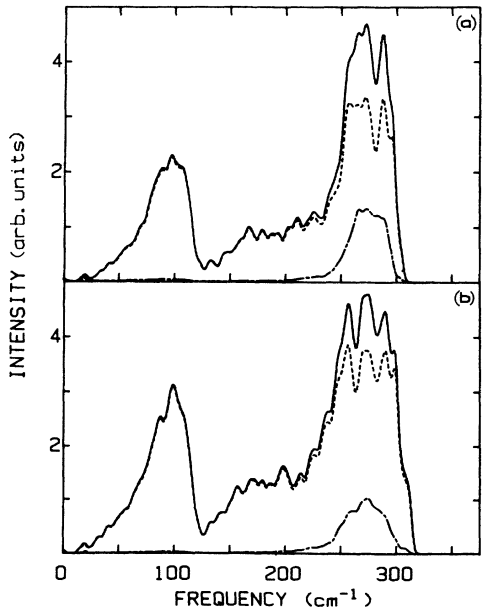

FIG. 10. Calculated *VH* reduced spectra (solid line) for Ge of models *B* (a) and *E* (b) and the contributions of mechanisms 1 (— — —) and 2 (— — —).

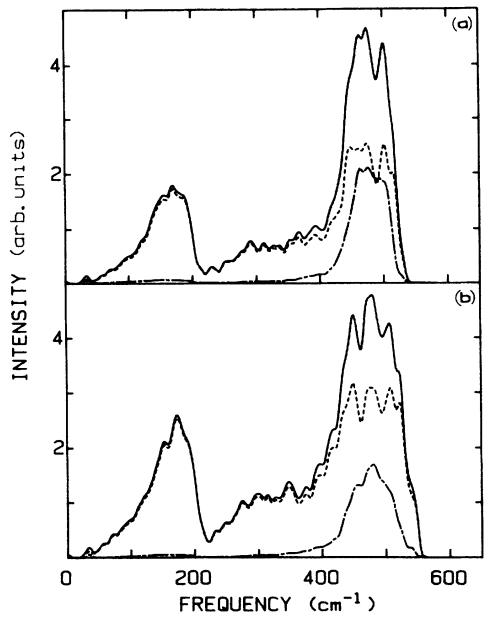

FIG. 11. Calculated *VH* reduced spectra (solid line) for Si models *B* (a) and *E* (b) and the contributions of mechanisms 1 (— · — · —) and 2 (— — —).

fit results, however, in a large increase in the $(B_1/B_2)^2$ values of Table III. This alternative fitting procedure substantially increases the contribution of the allowed $\tilde{D}_1$ mechanism to the scattering. While the results of Figs. 10 and 11 and Table III seem more plausible, further developments in the Raman scattering theory are clearly required to more precisely determine the relative value of the weighting coefficients for the individual $\tilde{D}_j$.

As Eqs. (2) and (3) indicate, measurements of the *HH* Raman component depend on contributions from all three mechanisms. The results of the FP analysis above indicate that the TA band intensity may not be employed to estimate the $\tilde{D}_3$ contribution here. For the TO band, the depolarization ratio, $dp(\mathrm{TO}) \equiv I_{VH}(\mathrm{TO})/I_{HH}(\mathrm{TO})$, at the peak may be utilized. With $dp(\mathrm{TO}) \simeq 0.55$, these equations and the relative strength of $\tilde{D}_3$ and $\tilde{D}_2$ of Table II yield $(B_3/B_2)^2$ of Table III. The results of Table III imply an approximate factor of 2–2.5 greater $\tilde{D}_2$ contributions to the *HH* spectra than the $\tilde{D}_3$ mechanism. The present results thus emphasize that within the current theory all three contributions to the Raman scattering need be included in the analysis of *HH* or unpolarized spectra.

The origin of the differences between the experimental and theoretical Raman spectra, especially the *VH* component, may have several possible sources. At lower frequencies, the differences between the FP experimental and theoretical spectra for the TA band as well as the behavior of $G(Q,E)$ also suggest possible limitations on the current *VH* theory in this region. Modification of the current theory may also influence the intermediate-frequency range. It is also possible that structural effects beyond short-range bond-angle disorder influence this frequency band. Recent theoretical work[22] has suggested that at intermediate frequencies, third neighbor, combined bend and stretch modes effects, rather than rings, may be of significance.

V. DENSITY OF STATES

The density of states of *c*-Ge obtained from $\beta/\alpha = 0.143$ is shown in Fig. 1, along with experimental data of Nelin and Nilsson.[19] Except for the TA band, good agreement exists, given the model simplicity. In Fig. 12, the $G(E)$ for two samples of highly ordered (HO) and highly disordered (HD) *a*-Ge are compared to the theoretical spectra obtained by averaging the results for the 500- and 519-atom models. The density of states of *a*-Ge was obtained from an appropriate average over Q of $G(Q,E)$. Figure 13 illustrates the $G(Q,E)$ spectrum obtained on the HO sample. The oscillatory behavior of $G(Q,E)$ exhibits dynamical correlation effects noted above. As in the case of the Raman spectra, models *B* and *E* are employed in the comparison with HO and HD samples, respectively. As the resolution of the neutron measurements was 3.9 meV, the theoretical spectra have been Gaussian broadened by this amount. The area normalized comparison, shown in Fig. 12, indicates relatively good agreement in the form and trends in the TA and TO peaks with disorder, given the simplicity of the two-parameter lattice-dynamical model. At intermediate frequencies, the LA shoulder is found to be a factor of ~ 1.5 greater in the experimental spectra. This similar behavior has also been observed[23] in *a*-Si, as well as in other theoretical models of $G(E)$.[6] One feature of the neutron spectra, namely the LO region shoulder at ~ 230 cm^{-1}, is found to be considerably better resolved than in either the calculated $G(E)$ or experimental Raman scattering components. Only in the case of highly disordered *a*-Ge is a distinct LO-like *VH* Raman feature observed. This implies that a coupling parameter effect results in a less

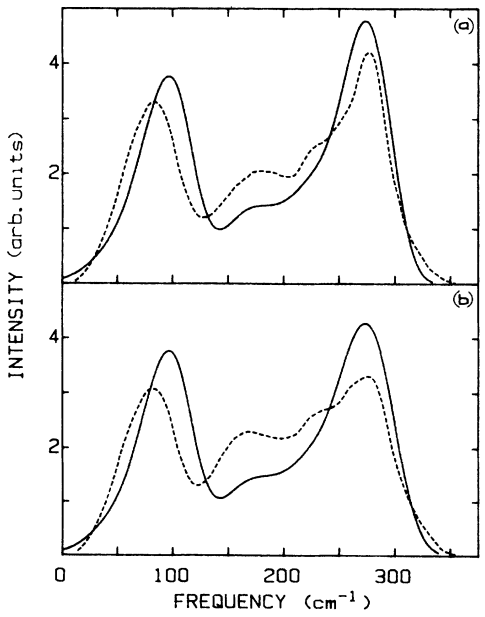

FIG. 12. Comparison between measured (— — —) and broadened calculated (——) phonon spectra: (a) HO sample and model *B* and (b) HD sample and model *E*. Spectra are area normalized.

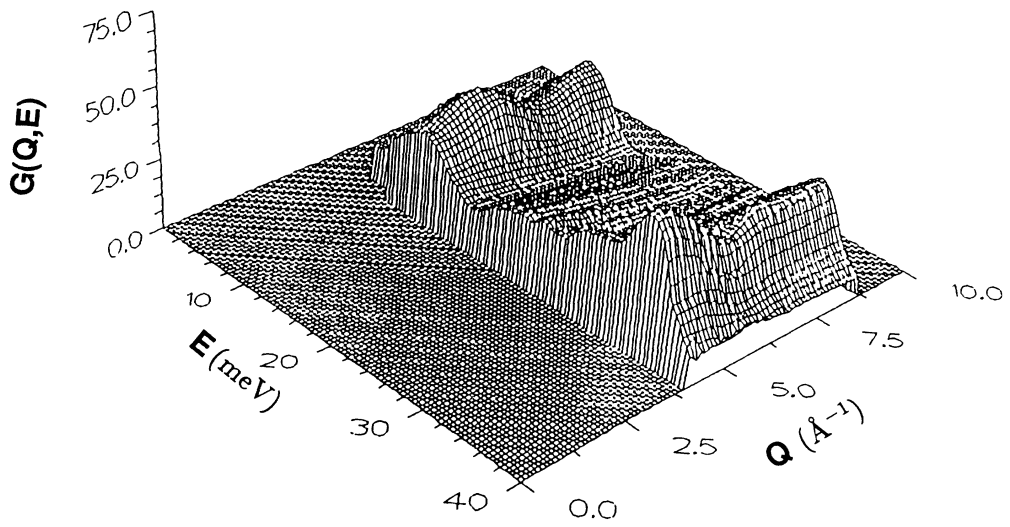

FIG. 13. $G(Q,E)$ spectrum of HO a-Ge sample.

discernible feature in the Raman than neutron spectra.

The experimental TO half-widths and lower-energy tail intensity of Fig. 12 are found to be larger than the theoretical results. Other structural models similarly yield narrower TO widths than that observed experimentally. It is possible that this is a consequence of a neglect of quantitative disorder related to local fluctuations in the force constants with bond-angle disorder. Variations from the tetrahedral bond angle are expected to reduce the strength of the bond-stretching interaction, resulting in an asymmetric broadening to lower frequencies. While the neglect of variations in force constants has generally been justified on the basis of similar first-neighbor distances, the sensitivity of the TO band to bond-angle disorder implies that quantitative disorder may also influence band shape. This might also explain the larger LO region shoulder observed experimentally. Possible evidence for such broadening may be seen in variations of the optical gap between samples of a-Ge and a-Si.[1] Similar local fluctuations in sp^3 orbital interactions that modify the optical gap would logically result in fluctuations in the bond-stretching force constant.

The density of states of the HD a-Ge sample is qualitatively similar to that obtained on a rf-sputtered a-Si.[23] The latter was prepared on an uncooled substrate at a pressure of 50 mTorr and is thus expected to also be moderately disordered when referenced to the a-Si anneal stable state. Both a-Ge and a-Si exhibit well-defined TA bands and minima as well as a broad TO band. If the spectra are scaled in energy to the TO peak, then the a-Si TA peak occurs $\sim 22\%$ higher in energy. This shift has been previously noted in Raman studies of a-$Ge_{1-x}Si_x$ alloys[1] and attributed to an increased bond-bending force constant in a-Si. While an earlier a-Si $G(E)$ spectrum[24] exhibited a more distinct peak in the LO region near 400 cm^{-1}, more recent measurements[23] indicate a form similar to that of a-Ge.

The addition of H to a-Si yields a hydrogen partial density of states that differs from that of a-Si for $\omega < 600$ cm^{-1}.[22] In particular, the TA intensity is substantially reduced in relative intensity. This result has been interpreted as indicating that the H does not passively move in phase with Si atoms during lower energy excitations. Recent Raman scattering measurements in rf-sputtered a-$Si_{1-x}H_x$ indicate, however, that the introduction of H into a-Si results in substantial changes in the TA- to TO-intensity ratio.[25] This is a consequence of both a narrowing of the TO band and a decrease in the TA band due to a reduction of the number of bond-bending modes. If, as suggested from the two a-Ge $G(E)$ samples, the coupling parameter is not a significant function of order or [H], then the observed decrease in the Raman TA- to TO-intensity ratio is primarily a result of changes in $G(E)$. As such, the H atoms appear to more nearly move as passive atoms at lower energies than previously suggested. This result is physically plausible given the strong Si—H bonding and the light H mass.

VII. STRUCTURAL ORDER

The very good comparison between the spectra for structural models B and E and the highly ordered and disordered a-Ge and a-Si films implies that the actual bond-angle distribution widths should be near to those of the models. This comparison utilized a fit to the experimental data from intermediate to high frequencies. It is also possible to independently compare the experimental and theoretical VH and FP TO half-widths to estimate the approximate range and values of the bond-angle distribution widths studied here. Figure 14 exhibits the theoretical dependence obtained for the TO widths for mechanisms $\tilde{D}_j$ on $\Delta\theta_G$. The solid and dashed lines are the fits obtained for the VH spectra to linear combinations of $\tilde{D}_1$ and $\tilde{D}_2$ mechanisms for samples a and d. As the theoretical width of the TO bands for the individual $\tilde{D}_j$ components is proportional to $\Delta\theta_G$, it is reasonable to

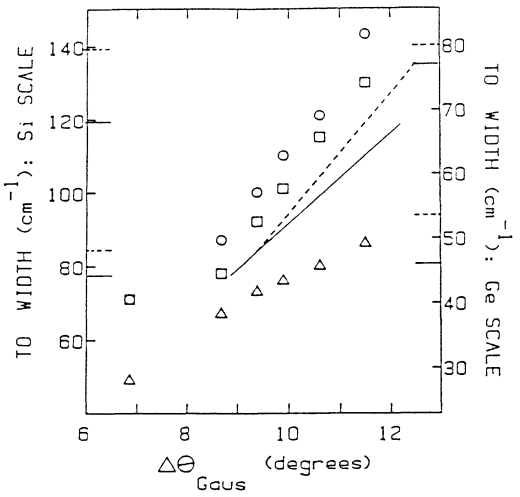

FIG. 14. Theoretical TO peak widths for mechanisms 1 (△), 2 (○) and 3 (□) as a function of $\Delta\theta_G$. Horizontal solid and dashed lines on Si and Ge axes mark the maximum and minimum Δ values experimentally observed for the depolarized and full polarized components, respectively. The solid and dashed diagonal lines are linear fits to the *VH* *a*-Si and *a*-Ge spectra, respectively.

assume a linear correlation between the experimental TO widths and $\Delta\theta_G$. With these assumptions, Table IV indicates the resulting estimates of the bond-angle widths for maximally and minimally order films, *a* and *d*, respectively, of *a*-Ge and *a*-Si. In addition, Table IV gives the value that would be obtained were the $\tilde{D}_1$ mechanism neglected. The independent estimates obtained from the FP and *VH* components are very similar. Table IV also indicates rather similar values for *a*-Ge and *a*-Si. The results, as noted earlier, clearly indicate that it is necessary to include the latter to explain the observed Raman spectra and the depolarization ratio.

For the highly disordered samples of *a*-Si and *a*-Ge the TO widths for the *VH* spectra exceed the widths of model *E* obtained from linear combinations of the $\tilde{D}_1$ and $\tilde{D}_2$ mechanisms. Similarly the FP width is somewhat larger than the $\tilde{D}_3$ mechanism results for model *E*. This is noted by the estimated $\Delta\theta_G$ of $\sim 12° \pm 0.2°$ obtained from a fit to the width of the TO band, which is somewhat greater than the 11.5° value of model *E*. In contrast, the model *B* fits to samples *a* agree well with the TO width. Further experimental studies of more highly disordered *a*-Si and *a*-Ge are thus required to more accurately determine the bond-angle disorder that may be obtained in practice. If the disorder in samples *d* is found to be greater than that of model *E*, then some small changes in the values of Table III are expected.

TABLE IV. Summary of the estimates of $\Delta\theta_G$ variation based on Fig. 14.

Raman components compared		$\Delta\theta_G$ (deg)			
		a	*d*	*a*	*d*
Expt.	Theor.	*a*-Si		*a*-Ge	
FP	3	9.0	12.0	9.5	12.0
VH	2	8.2	10.4	8.3	11.3
VH	1 + 2	8.9	12.2	9.2	12.4

The results of Table IV are in very good agreement with estimates of the range of bond angles for *a*-Ge obtained from extrapolations of RDF, optical-gap, and Raman scattering data.[1,21] Recent analysis of differential scanning calorimetry spectra on annealed states of low-temperature-ion implanted *a*-Ge have been utilized to estimate the variation of the rms values of the bond-angle distribution.[8] These calculations assume a quadratic dependence of the strain energy and heat of relaxation on the rms bond-angle width, as well as a similar dependence for the heat of crystallization. Utilizing the minimum value of $\sim 9°$ for $\Delta\theta_G$, yields a range of values comparable to that obtained here.

The values given in Table IV differ from previous estimates[2] of the bond-angle distribution width based on a comparison of polarization unanalyzed Raman spectra and the $\tilde{D}_2$ dependence on $\Delta\theta_G$. As Fig. 14 shows, neglect of the $\tilde{D}_1$ contribution yields lower limits to the value of $\Delta\theta_G$. The present results, which include all three $\tilde{D}_j$ mechanisms, yield larger values for the maximally ordered states of *a*-Ge and *a*-Si, as well as a smaller variation with disorder. This is also more consistent with differential calorimetry estimates of $\Delta\theta_G$ with annealing temperature.[8] Figure 14 indicates that inclusion of a $\tilde{D}_1$ contribution yields a less rapid variation of the TO width relative to that obtained from consideration of the $\tilde{D}_2$ mechanism alone. In addition, this result emphasizes that polarization analysis of the Raman scattering is necessary to obtain bond-angle deviation estimates. Recent resonance Raman studies have indicated that the TO width of the *HH* spectra is a function of the laser excitation frequency, while the *VH* width is relatively independent of excitation conditions.[26] As such, evaluation of structural disorder is more reasonably estimated from the *VH* component. It is perhaps useful to note that polarization unanalyzed Raman spectra, which are a mixture of *VH* and *HH* components that are spectrometer dependent, yield less accurate estimates of structural order.

VIII. CONCLUSIONS

The experimental results in both *a*-Ge and *a*-Si films indicate variations in the *VH* and *HH*-(4/3)*VH* Raman spectra that imply modifications of the basic Raman mechanisms with bond-angle disorder, This is confirmed by theoretical results on a systematic set of 500- and 519-atom models which indicate that inclusion of all three $\tilde{D}_1$ mechanisms is required to describe the Raman spectra. This is of importance particularly to Raman studies which do not analyze the scattered polarization and are mixtures of these components. The intensity of both the $\tilde{D}_2$ and $\tilde{D}_3$ components is found to vary quadratically as the rms bond-angle variation, while the $\tilde{D}_1$ contribution is structurally insensitive, as is physically reasonable.

A direct comparison between the FP spectra and the form of the $\tilde{D}_3$ component indicates differences at low en-

ergies that have been suggested to arise from current limitations of the theory. (It is alternatively possible that resonant Raman effects modify the FP spectrum in a manner not included in the current theory.) An analysis of the *VH* component, which is not resonance sensitive, provides information on the relative contributions of the $\tilde{D}_1$ and $\tilde{D}_2$ terms. Here, too, limitations exist in the current theory for low energies that suggest the need for a more detailed polarizability theory that involves two or more bond effects. At higher energies the experimental and theoretical results exhibit similar trends with bond-angle disorder. A comparison of the results for models with high and low degrees of disorder with *a*-Ge spectra yield very good agreement with other estimates of the bond-angle disorder. Similar variations in this measure of short-range structural order are also suggested for *a*-Si. Good agreement was also obtained between the experimental and theoretical phonon densities of states. Differences exist, however, in the band intensities at intermediate energies in the narrower TO bandwidth that suggest some limitations of the current Hamiltonian. The inclusion of quantitative disorder in the force constants due to bond-angle fluctuations may yet improve agreement.

ACKNOWLEDGMENTS

This work (J.S.L.) was supported by National Science Foundation (NSF) Grant No. NMR-86-20391.

---

*Present address: Coordinated Science Laboratory, University of Illinois at Urbana-Champaign 1101 West Springfield Avenue, Urbana, IL 61801-3082.

[1]J. S. Lannin, in *Semiconductors and Semimetals*, edited by J, I. Pankove (Academic, New York, 1984), Vol. 21B, p. 159.

[2]D. Beeman, R. Tsu, and M. F. Thorpe, Phys. Rev. B **32**, 874 (1985).

[3]N. Maley, J. S. Lannin, and H. Ugur, J. Non-Cryst. Solids **77/78**, 1073 (1985).

[4]J. S. Lannin, J. Non-Cryst. Solids **97/98**, 39 (1987).

[5]R. Alben, D. Weaire, J. E. Smith, Jr., and M. H. Brodsky, Phys. Rev. B **11**, 2271 (1975).

[6]D. Beeman and R. Alben, Adv. Phys. **26**, 339 (1977).

[7]D. Bermejo and M. Cardona, J. Non-Cryst. Solids **32**, 405 (1979).

[8]J. Fortner and J. S. Lannin, Phys. Rev. B **37**, 10 154 (1988).

[9]K. Sköld and D. Price, in *Neutron Scattering A*, Vol. 23 of *Methods of Experimental Physics* (Academic, New York, 1986).

[10]N. Lustig, J. S. Lannin, J. M. Carpenter, and R. Hasegawa, Phys. Rev. B **32**, 2778 (1985).

[11]N. Maley, J. S. Lannin, and D. L. Price, Phys. Rev. Lett. **56**, 1720 (1986).

[12]D. E. Polk and D. S. Boudreaux, Phys. Rev. Lett. **31**, 92 (1973); D. E. Polk, J. Non-Cryst. Solids **5**, 365 (1971).

[13]M. G. Duffy, D. S. Boudreaux, and D. E. Polk, J. Non-Cryst. Solids **15**, 435 (1974).

[14]R. J. Temkin, W. Paul, and G. A. N. Connell, Adv. Phys. **22**, 581 (1973).

[15]G. Etherington, A. C. Wright, J. H. Wenzel, J. C. Dore, J. H. Clarke, and R. N. Sinclair, J. Non-Cryst. Solids **48**, 265 (1982).

[16]P. Steinhardt, R. Alben, and D. Weaire, J. Non-Cryst. Solids **15**, 199 (1974).

[17]J. S. Lannin, in *Disordered Semiconductors*, edited by M. A. Kastner, and G. A. Thomas (Plenum, New York, 1987), p. 283.

[18]Y. C. Hsieh, J. Chem. Phys. **22**, 306 (1954).

[19]G. Nelin and G. Nilsson, Phys. Rev. B **5**, 3151 (1972).

[20]N. Maley and J. S. Lannin, Phys. Rev. B **35**, 2456 (1987).

[21]J. S. Lannin, N. Maley, and S. T. Kshirsagar, Solid State Commun. **42**, 197 (1982).

[22]C. S. Nichols, M. F. Ross, and C. Y. Fong, Phys. Rev. B **32**, 1061 (1985).

[23]W. A. Kamitakahara, C. M. Soukoulis, H. R. Shanks, U. Buchenau, and G. Grest, Phys. Rev. B **36**, 6539 (1987).

[24]H. R. Shanks, W. A. Kamitakahara, J. F. McClelland, and C. Carlone, J. Non-Cryst. Solids **59/60**, 197 (1983).

[25]N. Maley and J. S. Lannin, Phys. Rev. B **36**, 1146 (1987).

[26]M. Stutzman (private communication).